HHS Public Access

Author manuscript

J Neural Eng. Author manuscript; available in PMC 2020 August 08.

Published in final edited form as:

J Neural Eng. 2014 August ; 11(4): 046021. doi:10.1088/1741-2560/11/4/046021.

Effects of location and timing of co-activated neurons in the auditory midbrain on cortical activity: implications for a new central auditory prosthesis

Małgorzata M Straka[1], **Melissa McMahon**[1], **Craig D Markovitz**[1], **Hubert H Lim**[1,2,3]

[1]Department of Biomedical Engineering, University of Minnesota, Twin Cities 312 Church St SE, Minneapolis, MN 55455, USA

[2]Institute for Translational Neuroscience, University of Minnesota, Twin Cities Minneapolis, MN 55455, USA

[3]Department of Otolaryngology, University of Minnesota, Twin Cities 516 Delaware Street SE, Minneapolis, MN 55455, USA

Abstract

Objective.—An increasing number of deaf individuals are being implanted with central auditory prostheses, but their performance has generally been poorer than for cochlear implant users. The goal of this study is to investigate stimulation strategies for improving hearing performance with a new auditory midbrain implant (AMI). Previous studies have shown that repeated electrical stimulation of a single site in each isofrequency lamina of the central nucleus of the inferior colliculus (ICC) causes strong suppressive effects in elicited responses within the primary auditory cortex (A1). Here we investigate if improved cortical activity can be achieved by co-activating neurons with different timing and locations across an ICC lamina and if this cortical activity varies across A1.

Approach.—We electrically stimulated two sites at different locations across an isofrequency ICC lamina using varying delays in ketamine-anesthetized guinea pigs. We recorded and analyzed spike activity and local field potentials across different layers and locations of A1.

Results.—Co-activating two sites within an isofrequency lamina with short inter-pulse intervals (<5 ms) could elicit cortical activity that is enhanced beyond a linear summation of activity elicited by the individual sites. A significantly greater extent of normalized cortical activity was observed for stimulation of the rostral–lateral region of an ICC lamina compared to the caudal–medial region. We did not identify any location trends across A1, but the most cortical enhancement was observed in supragranular layers, suggesting further integration of the stimuli through the cortical layers.

margo.straka@jhu.edu.

Online supplementary data available from stacks.iop.org/JNE/11/046021/mmedia

Conflicts of interest

None.

Significance.—The topographic organization identified by this study provides further evidence for the presence of functional zones across an ICC lamina with locations consistent with those identified by previous studies. Clinically, these results suggest that co-activating different neural populations in the rostral–lateral ICC rather than the caudal–medial ICC using the AMI may improve or elicit different types of hearing capabilities.

Keywords

auditory cortex; deep brain stimulation; enhancement; inferior colliculus; temporal integration; neural implant

Introduction

Hearing loss has been treated with auditory prostheses such as the cochlear implant (CI) or auditory brainstem implant (ABI) for decades. By stimulating along the tonotopic gradient of the auditory nerve within the cochlea, the CI is able to provide temporal and spectral cues that are sufficient to understand speech [1–3]. For people without an implantable cochlea or functioning auditory nerve, ABIs have been used as an alternative to the CI. The primary group targeted for ABIs are patients with neurofibromatosis type II (NF2), a genetic disorder in which bilateral tumors develop along the auditory nerves. Unfortunately, ABIs typically result in poorer performance than CIs, particularly for NF2 patients [4–6], though the performance levels of some recent ABI patients have neared that of CI patients [7–9]. As an alternative to the ABI, the auditory midbrain implant (AMI) was developed with an array of 20 sites along a single shank for stimulating along the tonotopic gradient of the central nucleus of the inferior colliculus (ICC) [6, 10]. The AMI was implanted in five NF2 patients in 2006–2008. Although AMI stimulation has been shown to activate neurons in a frequency-specific manner and transmit spectral cues to higher auditory processing centers, the temporal coding abilities seem limited [11–15].

Calixto *et al* [16] investigated this AMI limitation by activating the ICC with the AMI array and recording the evoked activity in the primary auditory cortex (A1) of guinea pigs. They found that repeated stimulation of a neural population with a single AMI site within an isofrequency lamina of the ICC causes refractory and suppressive effects of local field potentials (LFPs) in layer III/IV of A1 on short (<10 ms) and long (>10–100 ms) time scales. These negative effects, which may have limited the temporal coding capabilities of AMI patients, could be overcome by stimulating multiple neuronal populations along an isofrequency lamina with dual site stimulation (DSS: two AMI sites within the same ICC lamina). Similar results were also seen for LFPs and spiking in supragranular, granular and infragranular layers across A1 in response to ICC stimulation with much smaller sites (413 μm^2 versus 126 000 μm^2) [17]. In addition, co-activating sites with short delays at less than 6 ms resulted in enhanced cortical activity (i.e., activity larger than the linear summation of activity induced by the individual sites), with the strongest enhancement in supragranular layers. Although cortical enhancement did not appear to be affected by the recording location across A1, preliminary data suggested that it was influenced by the stimulation location across an ICC lamina.

The location of stimulation across an ICC lamina is expected to impact cortical responses because specific ICC regions differ in physiological responses as well as anatomical inputs and outputs. Maps for response properties have been found across an isofrequency lamina, including for best modulation frequency, spike latency, spike jitter, binaural properties, threshold and tuning properties [18–27]. These different response properties across an ICC laminae may arise from differences in input and output projection patterns. Anatomical studies have found functional zones that are spatially distinct within the ICC as a result of different projections from the brainstem [28–32]. For example, in the gerbil two specific zones have been identified in the ICC corresponding to its rostral–lateral and caudal–medial regions that project differentially to rostral and caudal regions of the ventral division of the medial geniculate (MGV), respectively [33].

Differences in function across an ICC lamina are further supported by an electrical stimulation study, which found that activation of the rostral–lateral regions versus the caudal–medial regions of the ICC elicit different responses in A1 [34]. In contrast to the rostral–lateral regions, stimulation of the caudal–medial regions of the ICC required higher activation thresholds and elicited evoked potentials in A1 that are smaller in magnitude, have longer latencies and exhibit larger discriminable level steps. Since these cortical activation properties are evident when stimulating with individual pulses across an ICC lamina, cortical activity is also expected to vary with ICC location when co-activating multiple neuronal populations.

In this study, we investigated the relationship between cortical responses and the location of co-activating ICC neurons with DSS at short inter-pulse intervals (IPIs). By using fewer delays than in our previous study [17], we had sufficient time to stimulate more locations across an ICC lamina per animal to create a more complete location map. We also re-examined whether locations across A1 contributed to the differences observed in the extent of enhancement elicited with DSS. As with our previous study, we did not find a trend between the pattern of DSS-induced cortical activity and the recording location in A1. However, we found that stimulating rostral–lateral regions of the ICC with short IPIs led to stronger normalized cortical activity in contrast to caudal–medial regions, with the greatest enhancement occurring in the supragranular cortical layers.

Methods

Overview

Similar surgical procedures and methods for both stimulation and neural recording to previous work [12, 17, 35] were used and are briefly summarized below. Acoustic-driven responses were used to guide the placement of 32-site, silicon-substrate Michigan electrode arrays (NeuroNexus Technologies, Ann Arbor, MI) within the ICC and A1 of guinea pigs anesthetized with ketamine. We then used DSS by applying a single electrical stimulation pulse at each of two sites across a 10 kHz isofrequency ICC lamina, varying delays between the two pulses, and recorded corresponding LFPs and multi-unit spiking activity in A1. These experiments investigated how cortical activation throughout A1 varied when stimulating different neurons across an ICC isofrequency lamina.

Surgery

Experiments were performed on 13 male and female Hartley guinea pigs (387 ± 57 g, Elm Hill Breeding Labs, Chelmsford, MA) in accordance with policies of the University of Minnesota's Institutional Animal Care and Use Committee. An intramuscular injection of ketamine (40 mg kg^{-1}) and xylazine (10 mg kg^{-1}) was used to initially anesthetize the animals, and an areflexive state was maintained with periodic supplements. The animal was placed into a stereotaxic frame (David Kopf Instruments, Tujunga, CA) before the surgery, where the right side of the cortex was exposed from the rostral end of the temporal lobe to the caudal end of the occipital lobe. After removing the dura, the arrays were inserted into the ICC and A1 with micromanipulators. The exposed brain was then covered with agarose gel.

Stimulation and recording setup

All experiments were performed within a sound attenuating and electrically shielded chamber. Custom software written in MATLAB (MathWorks, Natick, MA) was used to control the computer interface with TDT System 3 hardware (Tucker-Davis Technology, Alachua, FL). Neural data was processed through analogue dc-blocking and anti-aliasing filters (1.6 Hz to 7.5 kHz). Acoustic stimulation was sampled at 195 kHz and neural recordings were sampled at 24 kHz. A speaker presented acoustic stimulation to the left ear through a hollow ear bar, and this system was calibrated with a 0.25 inch condenser microphone (ACO Pacific, Belmont, CA) and a short plastic tube that represented the ear canal. We electrically stimulated sites on the ICC array with current levels up to 100 μA using pulses that were biphasic, cathodic-leading, charge-balanced and 205 μs/phase. A monopolar configuration was used for electrical stimulation, with a ground return in the neck muscles. The ground needle for recording signals was placed either into the parietal lobe or under the skin ~2 cm rostral to the bregma, with no obvious differences in results between the two.

Placement of arrays

The position of the array within the ICC or A1 was confirmed online by plotting frequency response maps (FRMs) and post-stimulus time histograms (PSTHs) of spiking activity, similar to previous publications [12, 13, 36]. On each site, neural signals were bandpass filtered from 300–3000 Hz and spikes were detected when signals exceeded three standard deviations above the background activity. To create FRMs, pure tones of 1–40 kHz (8 steps/octave) were presented at levels from 0–70 dB (in 10 dB steps), with four trials of each stimulus. To calculate the best frequency (BF), we first visually determined the threshold, or the smallest stimulus level that elicited consistent spiking responses, and then determined the centroid of frequencies eliciting spiking responses at 10 dB above this threshold.

All array placements into A1 were confirmed by observing tonotopic shifts of high to low BFs from the dorsal-caudal to ventral-rostral locations [37]. The A1 array comprised four shanks that were 5 mm long and were separated by 400 μm. Each shank consisted of eight 177 μm^2 sites linearly separated by 200 μm. In order to align each shank along a cortical column, we inserted the array approximately perpendicular to the cortical surface [37–39]. For each shank, the average difference of BFs (ΔBF) between sites in layers I/II, III/IV and

V was 0.08 ± 0.08 octaves (mean ± SD), which is less than the local critical frequency scatter of up to 0.4 octaves that can be seen in isofrequency bands of A1 [40, 41]. The similarity in BF suggests placements may have been in one cortical column, though this was not confirmed with histology.

Cortical location effects were investigated using reconstructions of site locations created with images of array placements taken with a microscope (OPMI 1 FR pro, Zeiss, Dublin, CA). Site locations across animals were normalized using landmarks including the middle cerebral artery, major vasculature and bregma and lateral suture lines, similar to previous studies [37, 40, 42]. Only recording sites in A1 with BFs similar to the stimulated sites in the ICC were used in data analysis (ICC-to-A1 ΔBF: 0.2 ± 0.1 octaves), and these locations are shown in figure 1(a).

Similar to previous publications [16, 17], we identified A1 layers with current source density analysis [43–45] of activity in response to 100 trials of 70 dB SPL broadband noise. The site with the shortest latency current sink corresponded to the main input layer, which is layer III/IV in guinea pig [46, 47]. Layer V was identified by a site as a current source and was typically two electrode sites (or 400 μm) deeper than layer III/IV. Corresponding to two electrode sites shallower than layer III/IV, we combined supragranular layers as layer I/II.

The ICC array consisted either of four 8 mm long shanks or of two 10 mm long shanks. For both arrays, each shank was separated by 500 μm and consisted of 700 μm^2 sites that were linear separated by 100 μm. The ICC array sites were activated prior to the experiment with cyclic voltammetry, which enabled both recording and stimulation up to 100 μA [12, 48]. In order to align the array along the tonotopic axis, the array was inserted through the visual cortex [49, 50] at a 45° angle to the sagittal plane. The placements of arrays within the ICC were confirmed by observing FRMs with a consistent shift from high BFs at deeper sites to low BFs at superficial sites along a shank [12, 49]. In all placements, the shanks were aligned in the caudal to rostral direction.

Electrical stimulation parameters

We electrically stimulated two sites within the ICC that were 500 μm apart and responded with similar BFs, and characterized the corresponding LFP and spiking activity within A1 for layers I/II, III/IV and V. For each ICC pair, the average ΔBF between the stimulated ICC sites was 0.08 ± 0.06 octaves. Across all animals, the ICC sites had an average BF of 10.3 kHz ± 0.3 octaves. Both the 4BF between ICC pairs and the BF scatter across the lamina were less than 0.3 octaves, which has previously been shown to be the approximate bandwidth of an isofrequency lamina in cat [51] and rat [52]. Therefore, we analyzed how stimulation across the 10 kHz isofrequency lamina affected cortical activity, and the ICC locations were determined by histology (see Histological reconstructions section). Across 13 animals, we recorded activity in 117 A1 locations in response to stimulation of 28 ICC site pairs for a total of 248 stimulation cases (i.e., ICC-A1 stimulation-recording site pairs).

Electrical stimulation was randomly presented at varying levels and IPIs, with 20 trials per stimulus. The IPIs included 0 (simultaneous stimulation), 0.5, 1, 2, 4 and 8 ms. We stimulated one site with up to ten levels across a 12 dB range. For the other site, only two or

three levels were chosen due to time restrictions. Only levels that elicited A1 activity above threshold but below saturation levels for all IPIs were analyzed, with an average of ten levels per stimulation case.

Histological reconstructions

Prior to placement, the ICC array was dipped in a red stain (Di-I: 1, 1-dioctadecyl-3, 3, 3′, 3′-tetramethylindocarbo cyanine perchlorate, Sigma-Aldrich, St Louis, MO) to later identify array position within the ICC during histological analysis. Detailed description of the histological procedure, midbrain reconstruction, normalization, and approximation of frequency laminae is provided in a previous publication [53]. Briefly, the midbrain was fixed with 3.7% paraformaldehyde and cryosectioned into sagittal sections at 60 μm using a sliding microtome (Leica, Buffalo Grove, IL). Images of each slice were taken using a Leica MZ FLIII fluorescence stereomicroscope (Leica, Buffalo Grove, IL), a Leica DFC412 C Peltier cooled CCD camera, and Image-Pro software (MediaCybernetics, Bethesda, MD). A single reflection white light image using a variable intensity fiber optic light source (Fiber-Lit-PL800, Dolan-Jenner Industries, Boxborough, MA) was taken to determine the outline of each slice. Fluorescence images were later superimposed on the white light images for visualization of the reference and array shank points. The brain was then reconstructed in three dimensions using Rhinoceros (Seattle, WA), and the positions of the arrays were estimated by creating best fit lines through the points on individual slices.

The reconstructions for each brain were normalized to one standard brain using the curvature of the IC and the reference needle point at the intersection of the superior colliculus, thalamus and lateral extension from the IC. The 10 kHz lamina was approximated by creating a plane orthogonal to the average insertion angle of all best fit lines of each array placement. The depth of the lamina was determined by calculating the distance from the surface of the IC, where neurons do not respond to broadband noise, to locations where neurons respond with specific BFs from previously published data [53]. This distance was multiplied by a scaling factor to account for tissue changes due to the histological process.

The reconstructions of each ICC array placement, as well as the 10 kHz lamina, can be seen in figure 1(b) within the normalized brain. Figure 1(c) shows the DSS locations across the 10 kHz lamina. In order to provide information about the shape of the ICC, these DSS locations are shown along with locations found to be on the border or outside the ICC from other data acquired in the lab [20]. Locations were determined to be outside the ICC if the FRMs did not exhibit a systematic shift from low to high BFs for superficial to deeper sites along a shank. Locations were labeled ‘border’ if the FRMs showed broad tuning with orderly shifts, if tonotopic shifts were not observed across the whole shank, or if a neighboring shank (which was simultaneously recorded) was outside the ICC. From the border information shown here, we believe we have sufficiently stimulated throughout the ICC lamina while avoiding other subnuclei of the ICC. In order to analyze how cortical activity varied due to stimulation across an isofrequency lamina, we found the location of the midpoint between each pair of stimulated ICC sites, or the midpoint location. The midpoint locations for all DSS sites are shown with the border points in figure 1(d).

Data analysis

Evoked potential activity.—Analysis of evoked potentials and spiking activity was similar to previous studies [17]. Briefly, only one response was present for the IPIs used (up to 8 ms). After the electrical artifact was removed from each trace, the LFP traces were averaged across trials and the area of the LFP was calculated. To calculate the area, we first formed a horizontal line connecting two points: the first on the baseline activity immediately preceding the deflection of the LFP and the second on the rising portion of the LFP (i.e., with the same *y*-value as the baseline activity). A trapezoidal function was used to calculate the area of the LFP underneath this horizontal line. To reduce variability, we removed trials where large sporadic activity was observed before the stimulus-driven activity (see [17] for details). Briefly, we compared each of the 20 traces to an averaged trace within 25 ms sliding windows. If the difference between the slope of an individual trace and the average slope within a window exceeded three standard deviations, the trial would be removed. For each stimulation case and level, at least 14 trials and an average of 17 trials were included in the LFP area calculation.

Spiking activity.—Spikes were detected offline by filtering signals from 300 to 3000 Hz after removal of the electrical artifact. For all trials analyzed in the LFP area calculation, the spiking rate was determined by summing spikes within a 45 ms window following the electrical stimulus onset. The driven spike rate (DSR) per trial was calculated by subtracting from this spike rate the spontaneous rate, which was determined using the 20 ms window preceding the electrical stimulus.

The first spike latency (FSL) was calculated by computing the mean latency of the first spike across all 20 trials. The minimum latency for a given trial was at least 3 ms after the onset of the electrical stimulus, which was the shortest latency based on visual inspection of all our data and is consistent with the difference between the minimal latency of ICC at ~4 ms [19, 54] and of A1 at ~7 ms [55]. If the first spike for a given trial did not occur within 45 ms (i.e., the window also used for DSR calculation), it was counted as a ‘miss’ and that trial was not included.

Layer V often had putative antidromic spiking activity. Antidromic activity was determined due to its short latencies, low temporal jitter, isolated activity predominantly in layer V where output neurons originate and a sudden change from little to robust spiking with only a minor increase in current level above threshold [35]. Due to the difficulty of isolating antidromic spikes from the multiunit orthodromic activity, this paper includes analysis for LFP areas but not spiking characteristics (DSR or FSL) for layer V.

Normalization.—In order to normalize LFP and DSR responses at each IPI, we divided the responses to DSS by the algebraic mean of the responses to stimulation applied separately at each of the two sites comprising the DSS. Normalized values above one (i.e. activity greater than a linear summation of activity elicited at the two sites individually) were considered enhanced.

Statistical tests.—Normalized, level-averaged cortical responses were fit to a mixed model using the nlme library in R [56], where the factors included the IPI, ICC location, A1

location, A1 layer and stimulation order (whether the rostral ICC site or the caudal ICC site was stimulated first). The random variable for the model was the animal from which data were collected. Significance was determined when $P < 0.05$ after a Holm–Bonferroni correction. Comparisons within significant factors, such as between A1 layers or comparing specific IPIs to the 8 ms IPI, were made using Wilcoxon signed-rank tests after applying a Holm–Bonferroni correction, unless otherwise specified.

Two significant factors in the mixed model included the caudal-rostral and medial-lateral directions across the ICC. In order to quantify the directionality of this location effect, response properties were fit to the midpoint of the locations of ICC stimulation pairs using two-dimensional, linear multiple regression analysis. The model determined the slope parameter here called the steepest gradient axis (i.e., the vector of greatest increase) for each response parameter.

Results

Typical cortical responses to DSS

Cortical responses varied depending on the delay between two pulses delivered to two different neural populations within a single ICC isofrequency lamina. Figures 2(a) and (b) show that both LFPs and spiking across cortical layers increase as the IPI decreases in response to DSS at one stimulation level, as previously shown [17]. The extent of the increase in activity was greater for layer I/II compared to the other layers for LFPs and spiking. Responses were quantified as LFP areas or DSRs (figure 2(c)) and then normalized to the sum of individual responses (figure 2(d)) to determine IPI curves. These curves indicate the effect of IPI on normalized responses at a single stimulation level for one stimulation case (i.e., an individual A1-ICC pair from one animal). These IPI curves reveal that at short IPIs, DSS can elicit enhanced cortical activity greater than a linear sum of the individual responses, indicated by a normalized value of one. In addition, the normalized values in the IPI curves highlight the difference between layers, showing that the superficial layers elicit stronger activity at short delays than the deeper layers. Though many stimulation levels were used, obvious level trends were not observed for levels that were above threshold and below saturation. Therefore, we averaged across these levels to determine IPI-a curves, as shown in figure 3. Accurately capturing the response for each stimulation case, the IPI-a curves were used in the following section to compare activity across locations in A1 and ICC.

To determine which factors played a significant role in cortical enhancement, we fit all of the IPI-a responses to a linear mixed model. In this model, the factors included IPI, ICC location, A1 location, A1 layer, stimulation order (whether the rostral or the caudal ICC site from the stimulation pair was stimulated first) and the random variable was the animal used in the data. Significant factors in this model included the medial to lateral direction ($P < 0.004$) and the rostral to caudal direction ($P < 0.002$) across the ICC lamina, the IPI ($P < 3 \times 10^{-16}$) and the cortical layer ($P < 3 \times 10^{-16}$). In addition, the stimulation order was significant ($P < 0.003$), and therefore we treated each order as independent stimulation pairs. Across A1, neither the medial to lateral nor the rostral to caudal direction was significant ($P > 0.05$). In the following sections we further investigate these location effects across the ICC

and A1 in order to better understand potential mechanisms influencing the enhancement effect.

Responses vary between different cortical layers

Normalized cortical responses varied significantly across cortical layers. Figure 4 shows the IPI-a curves for DSR and LFP activity across each cortical layer averaged across A1 and ICC locations. For all curves, it is evident that activity increases as IPIs decrease. For LFPs and DSRs recorded at each layer, we found that normalized cortical activity at the 0–4 ms IPIs was significantly larger than the cortical activity recorded at the 8 ms IPI ($P < 5 \times 10^{-8}$) and exceeded a value of one (i.e., greater than the sum of individual pulses). Therefore, the average cortical activity is enhanced at shorter IPIs for all layers. When comparing between layers, normalized IPI-a curves for both LFP areas and DSRs appear larger in supragranular layers than deeper layers at shorter IPIs in figures 4(a) and (b), respectively. LFP activity in layer I/II was significantly greater than that recorded in layer III/IV or layer V for 0–4 ms IPIs ($P < 0.005$). No significant differences were detected between LFPs recorded in layer III/IV and layer V. In addition, DSR activity recorded in layer I/II was significantly larger than that recorded in layer III/IV for 0–8 ms IPIs ($P < 0.01$). Therefore, enhancement was found at all layers, with a greater increase in cortical activity at short IPIs in the supragranular layer.

Responses vary across an ICC lamina

Next, we investigated how cortical responses vary depending on the stimulation location across the ICC lamina. Figure 5 highlights a case example of DSS on pairs of sites across the ICC eliciting different cortical responses when recording from one layer III/IV location in A1 in one animal. Figure 5(a) shows the midpoint location of four pairs of sites that were stimulated (symbols) along with the rest of the DSS stimulated sites (empty circles) for reference. Stimulation of the most caudal–medial pair of sites (pair #1) did not elicit activity at this cortical location within the current injection limits for safety and stability of our electrode arrays. The most caudal–medial region has previously been shown to require much higher thresholds to activate A1 [34], and therefore our inability to activate A1 was not unexpected. For the other stimulation pairs, we found electrical stimulation levels that elicited similar cortical activity at the 8 ms IPI and then plotted the IPI curves for those stimulation levels (figure 5(b)). Figure 5(b) shows that the cortical activity at shorter IPIs remains constant for pair #2, while it increases for the site pairs that are located in more rostral–lateral locations. The fact that the difference in cortical activity at short IPIs varies with ICC locations, despite the similarity in activity at longer IPIs, suggests that this is not a result of a threshold effect limiting cortical activity. Instead, this difference in activity at short IPIs is indicative of a property specific to the ICC stimulation location. The IPI-a curves in figure 5(c) further confirm that greater normalized cortical activity occurs due to stimulation of more rostral sites across all valid stimulation levels. This example shows that, when recording in a single cortical location, the ICC site pairs located in more rostral–lateral across the lamina elicited larger cortical activity at short IPIs than the site pairs located in more candal-medial regions.

To investigate this location effect across all animals, we plotted how the cortical response at specific IPIs varied with the locations of the stimulated ICC site pairs (i.e., the midpoint location of the site pairs). Figure 6(a) shows that the normalized LFP responses to the 0 ms IPI are weakest in the caudal–medial region and strongest in the rostral–lateral region for all cortical layers. In order to quantify this directionality, we fit responses to ICC locations using two-dimensional, linear multiple regression analysis and found the steepest gradient axis (black lines in figure 6(a)), or the vector at which the responses increase the most. Next we plotted how the normalized LFP area varies across the steepest gradient axis (figure 6(b)). We collapsed the data along the caudal–medial to rostral–lateral axis, with 0 corresponding to the most caudal–medial point. Since several cortical locations could be recording activity from a single stimulation pair, cortical activity was averaged across all relevant recording locations. We found that the normalized cortical activity was smallest in the caudal–medial region of the ICC and increased towards the rostral–lateral regions. As shown in figure 7, similar trends were observed for normalized DSR across the ICC at the 0 ms IPI. In this paper, we show the 0 ms IPI map because the greatest amount of normalized cortical activity and thus the clearest trends were observed. Similar trends were observed for the 0.5 ms IPI and more diverse maps were observed for longer IPIs (data not shown, see summary in supplementary table 1, available from stacks.iop.org/JNE/11/046022/mmedia). The angle of the steepest gradient axis for LFPs and DSRs at each layer and IPI as well as descriptive statistics can be found in supplementary table 1.

In summary, we found significant fits at the 0 and 0.5 ms IPI for LFP at all layers and DSR for layer I/II (P <0.05). For DSR at layer III/IV, significant fits were found for the 0 ms IPI (P < 0.05). The average steepest gradient angles were generally similar for DSRs and LFPs, with an average of 57 ± 31° for LFPs and 78 ± 20° for DSRs for both IPIs (where 90° would be aligned with the caudal to rostral axis and 0° would be aligned with the medial to lateral axis). Differences in angles between LFP and DSR activity could be due to the limited spatial resolution of LFPs, since LFP activity reflects a large neuronal population that can span a distance of hundreds of microns whereas multi-unit spiking activity corresponds to a spatial span of tens of microns [44, 57–59]. Despite these differences, we found consistent trends for both LFPs and DSRs, where normalized cortical activity was small in the caudal–medial regions and much larger in rostral-medial regions. Combining LFP and DSR activity together, the average angle of the steepest gradient axis, or average steepest gradient angle, was 71 ± 20° across the 0 and 0.5 ms IPIs. Therefore, we conclude that DSS in rostral–lateral regions of an ICC lamina results in greater cortical activity in comparison to caudal–medial regions.

Responses in different A1 locations

Although the mixed model did not find significant trends that responses to DSS varied across A1 locations, we wanted to further investigate whether cortical locations played a subtle role. First, we determined whether responses to caudal–medial versus rostral–lateral ICC locations were evenly sampled throughout A1. With this aim, we found the line perpendicular to the average steepest gradient angle (i.e., perpendicular to the 71° line defined above). This line separated the ICC into rostral–lateral and caudal–medial regions, each with an equal number of stimulation locations (figure 8(a)). A1 locations for each

stimulated ICC location appeared to be evenly spread across A1 (figure 8(b)). This was further confirmed when comparison tests did not find a significant difference between the cortical locations recording activity elicited from caudal–medial versus rostral–lateral ICC regions (using a two-sided Wilcoxon rank sum test, $P > 0.05$). Because these locations were similarly distributed across A1, we could further investigate trends across the cortex. Since several ICC stimulation locations were recorded per A1 site, we found the mean cortical activity for each delay at each A1 site by averaging across all relevant ICC stimulation locations. Figure 9 shows the mean LFP or DSR activity recorded in layer I/II, III/IV or V for each cortical location at the 0 ms IPI. Confirming the results from the statistical model, we did not find trends of increased or enhanced activity across the cortex for the 0 ms or other IPIs (data not shown).

Latency

The previous results showed that, in response to DSS at short IPIs, normalized cortical activity was greater in supragranular than granular layers of A1. In order to better understand the mechanism involved in this increased supragranular activity, we calculated the mean FSL of each stimulation case for both A1 layers. The mean FSL was determined by averaging FSL across the same stimulation levels as the normalized LFP areas and DSRs above. We found the mean FSL was ~8 ms across all layer III/IV sites and ~11 ms across all layer I/II sites, as shown by histograms in figures 10(a) and (b), respectively. For A1 placements from which both layer I/II and layer III/IV sites were recorded, we calculated the difference between the FSL at layer I/II and layer III/IV and found this ΔFSL to be 3.3 ± 3.2 ms for the 0 ms IPI, as shown in figure 10(c). This ΔFSL value was consistent for all IPIs, with no trends between ΔFSL and IPIs. Thus, the distribution of latencies for the 0 ms IPI (figure 10(c)) was similar to the distribution of latencies for all IPIs (figure 10(c)).

Discussion

Stimulation of two different neural populations across the same ICC lamina elicits increased A1 activity across layers I–V at IPIs shorter than 4 ms. This time window agrees with previous studies where a ~6 ms window was determined when using more IPIs [16, 17]. Here we also found that the increased A1 activity greatly depends on the stimulation location across an ICC lamina, in which caudal–medial regions corresponded to no or small increases in activity while rostral–lateral regions resulted in greater normalized activity and even enhancement. Finally, we found that the greatest normalized activity and enhancement was found in supragranular layers. We did not observe any trends between the extent of normalized cortical activity and enhancement and the recording location across a given layer of A1. These results support the existence of a mechanism for enhancement within the pathway from the ICC to A1 that can functionally integrate activity across different neural populations within ICC on a fast temporal scale of less than 6 ms and that varies depending on stimulation location across an ICC lamina.

Anesthesia effects

In our study, we used an anesthetized preparation in order to position the electrode array into multiple ICC locations for each animal. We selected ketamine as the anesthetic because it is

thought to suppress the auditory cortex to a lesser extent than other anesthetics, particularly pentobarbital [60, 61]. Ketamine has been shown to affect cortical activity by reducing spontaneous activity [62, 63], inhibiting sound-evoked responses [62–64] and altering temporal processing in response to electrical stimulation of the cochlea [65]. Particularly at medium anesthesia depths, ketamine induces strong oscillatory responses in the auditory cortex [66–68], which results in greater variability to sound-evoked responses [66]. While trials with aberrant activity were removed to minimize the effect of these bursts, some of our location analysis may have been confounded by the variability in cortical responses, especially at longer IPIs. Despite these cortical effects, ketamine is unlikely to be the primary cause of the increased normalized cortical activity or enhancement observed at short IPIs when stimulating two sites within the same ICC lamina with DSS, since neither were previously observed [17] when repeatedly stimulating a single site or when stimulating two sites in different isofrequency laminae of the ICC using a similar stimulation and anesthesia protocol as in our study.

Possible neural mechanisms of cortical enhancement

It is unlikely that current summation or antidromic activation caused the increased normalized cortical activity or enhancement effects observed with DSS. While overlapping current fields at short IPIs can result in current summation, increased activity at or longer than 0.5 ms IPI cannot be only due to current summation because increased cortical activity at these longer IPIs was not observed during co-activation of two sites in different frequency laminae with a protocol similar to DSS in a previous study [17]. Moreover, current summation would be expected to result in greater cortical activity when stimulating in caudal–medial regions, which had higher thresholds, and thus required greater stimulation levels than rostral–lateral regions. In contrast, we found that the caudal–medial regions elicited less cortical activity than rostral–lateral regions at short IPIs. In addition, it is possible that antidromic activity could contribute to or alter enhancement of cortical activity, since the antidromic activation of corticofugal axons in the ICC could possibly activate axon collaterals that project from layer V up to superficial layers [69]. However, we had previously shown [17] that weaker and not greater normalized cortical activity was observed in granular or supragranular layers when antidromic activity was detected in layer V, and therefore concluded that it is unlikely that antidromic activity is the primary cause of the enhancement to DSS.

When stimulating with short IPIs, increased and even enhanced activity in A1 was observed in layer III/IV LFPs and DSRs, which corresponds to the synaptic input from MGV and neural output from A1 layer III/IV, respectively. Enhanced activity was also observed in LFPs and DSRs throughout the other cortical layers. The fact that the enhancement was seen at inputs and outputs across cortical layers supports the hypothesis that responses across an ICC lamina may be integrated by tectothalamic, thalamocortical, and/or corticocortical pathways.

The increased and enhanced activity observed at the synaptic input into A1 layer III/IV could arise either from the excitation of a greater number of MGV neurons or individual MGV neurons firing in a burst mode [70, 71]. In the visual system, a much larger cortical

response compared to that elicited from a single activation of a thalamocortical neuron can be elicited if two thalamocortical neurons are activated within a ~7 ms window or if the same thalamocortical neuron is re-activated within a ~15ms window [72]. The similarity of time windows (~7 ms for two neurons versus ~5 ms in our study), as well as the fact that most MGV neurons in ketamine-anesthetized guinea pigs respond with individual spikes rather than bursting patterns [73, 74], suggests that the enhancement seen in layer III/IV LFPs may be due to activation of a larger population of MGV neurons through stimulation of a greater number of tectothalamic neurons using DSS.

The supragranular cortical layers exhibited the greatest amount of normalized cortical activity enhancement, which may be due to non-lemniscal thalamocortical lemniscal thalamocortical, or corticocortical projections. Non-lemniscal projections could prime or enhance activity in supragranular layers via fast, large axons that principally originate in the medial division of the MGV [46, 75]. However, since these axons are so large that they may provide the earliest information to the cortex [46], the longer spiking latencies (by ~3 ms; see figure 10) in supragranular layers as compared to granular layers suggest that these non-lemnisical projections are unlikely to cause the increased cortical activity. In addition, the ΔFSLs were similar across all IPIs, despite the fact that greater normalized cortical activity was observed in supragranular versus granular layers only at short IPIs (i.e., less than 4 ms). The lack of IPI effects demonstrates that the ΔFSLs are independent of the amount of normalized cortical activity, at least at these suprathreshold levels. Instead, it seems likely that the transmission time between layer III/IV and layer I/II is on average ~3 ms, and that the increased enhancement in supragranular layers is due to mechanisms with longer latencies than the enhancement seen in granular layers. For example, the collaterals of tonotopic thalamocortical projections could prime the supragranular layers [46, 76, 77] or responses across granular layers could be integrated by the supragranular layers to lead to enhancement. Horizontal projections within supragranular layers [78] could also affect lateral inhibition even at distant cortical locations [79], and thus alter timing and integration of spiking activity. In addition, supragranular layers may incorporate multiple pathways, since supragranular layers are thought to integrate thalamocortical and corticocortical information before delivering it to corticofugal neurons in layers V and VI [77].

Differences in caudal–medial versus rostral–lateral regions in the ICC

We found little or no increased normalized cortical activity when co-activating sites with short IPIs in the caudal–medial region but strong cortical activity and even enhancement in the rostral–lateral region. When electrically stimulating single ICC sites and recording evoked responses in A1 in a previous study [34], the caudal-dorsal ICC region (which is equivalent to the caudal–medial region along a tilted ICC lamina in this study) achieved higher thresholds, larger discriminable level steps and smaller evoked potentials than the rostral-ventral region. However, it is unlikely that activation properties alone caused differences in cortical activity because rostral–lateral regions had much larger amounts of normalized cortical activity than caudal–medial regions at short IPIs even when both produced similar amounts of activity within A1 at the 8 ms IPI (figure 5(b)). Instead, it appears that the mechanism that results in increased cortical activity and enhancement, whether at the tectothalamic, thalamocortical, or corticocortical level, exhibits different

neural integration properties depending on the location of electrical stimulation across an ICC lamina.

In addition to differences in neural integration properties, several studies from our lab have shown systematic differences in response properties between the caudal–medial and rostral–lateral regions across an ICC lamina. In response to pure tones, neurons in the rostral–lateral versus caudal–medial regions of the ICC responded with shorter first spike latencies, less spiking jitter, larger LFPs that occur earlier and PSTHs that are shorter in duration and have more predominant onsets [20]. In another study, electrical stimulation of A1 elicited descending excitatory activation in the caudal–medial ICC but with minimal activation within the rostral–lateral ICC [80]. Since these studies were performed with similar histological reconstruction techniques to this DSS study, we normalized all midbrains and array placements onto a common standard brain (figure 11) to determine if these regions were consistent across studies. We found that the rostral–lateral region, which elicited increased or enhanced cortical activity for DSS (figure 11(a)), responded to pure tones with shorter PSTH durations (figure 11(b)), and with differences in other response features corresponding to greater spatial and temporal synchrony. In addition, little to no activity was present in these rostral–lateral regions in response to electrical stimulation of A1 (figure 11(c)). In contrast, caudal–medial regions, which elicited little or weak cortical enhancement in this study, typically responded to acoustic stimuli with weaker temporal and spatial synchrony, often responded to electric stimulation of A1.

In order to map locations across a given ICC lamina, we targeted only the 10 kHz lamina in this study and therefore cannot claim that these two identified regions exist throughout all ICC laminae, which roughly span 50 Hz-50 kHz in guinea pig [81, 82]. However, a previous study in guinea pig has shown similar spatial segregation of activation properties from the ICC up to A1 for different frequency laminae spanning 9–23 kHz [34]. In addition, segregated caudal–medial versus rostral–lateral ICC regions were anatomically demonstrated throughout low, middle and high frequency regions in gerbil [28, 33]. In response to electrical stimulation of A1, descending projections elicited activity in caudal–medial but not rostral–lateral regions for low, middle and high frequency lamina spanning from 2 to 16 kHz [80]. Finally, caudal–medial versus rostral–lateral regions have been shown to exhibit differential properties in response to pure tones at the 10 kHz and 20 kHz laminae [20]. Considering the consistency in ICC location trends across frequency regions for these different studies, we expect that the different DSS activation properties between the caudal–medial and rostral–lateral regions would also occur in the other isofrequency laminae throughout the ICC.

Subprojection pathway hypothesis

We have found that DSS of the rostral–lateral and caudal–medial regions across an ICC lamina result in different degrees of normalized cortical activity. While the normalized cortical activity appears to vary somewhat linearly between these two regions, this is likely because the location analysis was performed on the midpoint locations between each pair of sites (i.e., one site on each shank) that were 500 μm apart along an ICC lamina, resulting in spatial smearing. A previous study analyzing cortical responses to individual pulses

presented to the ICC found nonlinear trends between these two regions [34], suggesting the existence of at least two distinct clusters between the caudal–medial versus rostral–lateral regions. Two distinct clusters corresponding to these regions were also observed for maps of spiking response features to pure tones [20] as well as differences in corticofugal responses to electrical stimulation of A1 (see figure 11(b)).

These differences between regions across an ICC lamina are likely due to differences in input and output projection patterns that are maintained through the ascending lemniscal system. Anatomical studies in gerbil have shown that the caudal–medial and rostral–lateral regions of the ICC receive different inputs from the brainstem and project differentially to the caudal and rostral areas of the MGV, respectively [28, 33]. The anatomical segregation of the MGV is also continued in thalamocortical outputs, as demonstrated by studies in the cat and rat, which found that the rostral MGV projects throughout the auditory cortex, including A1, whereas the caudal MGV projects to core cortical regions predominantly outside A1 [83–87]. These segregated thalamic and cortical areas reveal differences in acoustic response properties similar to those observed in the ICC. In comparison to caudal regions, the neurons in rostral MGV respond to acoustic stimuli with stronger excitatory activation, shorter latencies with less jitter, more precise timelocking to click trains, and stricter tonotopic organization with narrower tuning curves [83]. The cortical regions that receive inputs from caudal MGV neurons typically exhibit responses with longer latencies, greater spiking jitter, less excitatory activity and less precise tonotopic organization compared to A1 regions, which receive inputs from rostral MGV neurons [83–88].

The differences in projection patterns from the brainstem and up to the cortex have led to the hypothesis that at least two subprojection pathways exist in the lemniscal system. Across the lemniscal nuclei, these response properties of the ‘rostral’ pathway suggests it may be designed for stronger activation and more precise transmission of sound information to higher centers in comparison to the caudal pathway. At least in the ICC, electrical stimulation of the A1 results in excitatory activation only in the caudal–medial region [80]. Combined with the more robust and precise activation properties identified for the rostral pathway, these findings suggest that the rostral pathway may serve as the main ascending pathway for transmitting sound cues to higher perceptual centers while the caudal pathway, at least within the midbrain, may serve a more modulatory and integrative role with the rostral neurons.

Conclusion

In this study, we have shown that co-activating neural populations across an ICC isofrequency lamina overcomes suppressive neural effects observed when repeatedly stimulating an individual site. To utilize this strategy in patients with the goal of improving speech perception, the second generation of the AMI will consist of two parallel linear arrays in order to stimulate along as well as within the isofrequency axis. As shown by this study, stimulating the more rostral–lateral region will likely lead to better cortical activation at short IPIs than caudal–medial regions, and therefore the rostral–lateral region appears to be a favorable target for implantation. Although greater normalized cortical activity was elicited when co-stimulating the rostral–lateral region of the ICC, clinical trials will still

need to be performed to determine whether this stimulation strategy and implantation location actually leads to improved speech understanding. In addition, future research should explore co-activating across ICC laminae with other stimulating strategies. For example, using bipolar stimulation in a single shank AMI has been shown to alter cortical thresholds and dynamic range, depending on the spacing between the stimulation and reference electrodes [86]. Combining bipolar stimulation with co-activation of neurons along an ICC lamina may lead to improved discrimination of temporal and frequency features, which in turn could lead to improved speech understanding.

Supplementary Material

Refer to Web version on PubMed Central for supplementary material.

Acknowledgements

We would like to acknowledge Robert Hughes for his contributions in the histological reconstructions. This work was supported by start-up funds from the University of Minnesota and NIH NIDCD R03DC011589.

References

[1]. Zeng FG 2004 Trends in cochlear implants Trends Amplif. 8 1–34 [PubMed: 15247993]

[2]. Shannon RV, Zeng FG, Kamath V, Wygonski J and Ekelid M 1995 Speech recognition with primarily temporal cues Science 270 303–4 [PubMed: 7569981]

[3]. Kral A and O'Donoghue GM 2010 Profound deafness in childhood N. Engl. J. Med 3 1438–50

[4]. Colletti V, Shannon RV, Carner M, Veronese S and Colletti L 2009 Progress in restoration of hearing with the auditory brainstem implant Prog. Brain Res 175 333–45 [PubMed: 19660666]

[5]. Schwartz MS, Otto S, Shannon RV, Hitselberger WE and Brackmann DE 2008 Auditory brainstem implants Neurotherapeutics 5 128–36 [PubMed: 18164492]

[6]. Lim HH, Lenarz M and Lenarz T 2009 Auditory midbrain implant: a review Trends Amplif. 13 149–80 [PubMed: 19762428]

[7]. Sennaroglu L et al. 2011 Auditory brainstem implantation in children and non-neurofibromatosis type 2 patients: a consensus statement Otol. Neurotol 32 187–91 [PubMed: 21224730]

[8]. Colletti L, Shannon R and Colletti V 2012 Auditory brainstem implants for neurofibromatosis type 2. Curr Opin Otolaryngol. Head Neck Surg 20 353–7 [PubMed: 22886036]

[9]. Matthies C et al. 2013 Auditory brainstem implantation improves speech recognition in neurofibromatosis type II patients ORL J. Otorhinolaryngol. Relat. Spec 75 282–95 [PubMed: 24042846]

[10]. Lim HH et al. 2007 Electrical stimulation of the midbrain for hearing restoration: insight into the functional organization of the human central auditory system J. Neurosci 27 13541–51 [PubMed: 18057212]

[11]. Lim HH, Lenarz T, Joseph G, Battmer RD, Patrick JF and Lenarz M 2008 Effects of phase duration and pulse rate on loudness and pitch percepts in the first auditory midbrain implant patients: comparison to cochlear implant and auditory brainstem implant results Neuroscience 154 370–80 [PubMed: 18384971]

[12]. Lim HH and Anderson DJ 2006 Auditory cortical responses to electrical stimulation of the inferior colliculus: implications for an auditory midbrain implant J. Neurophysiol 96 975–88 [PubMed: 16723413]

[13]. Lenarz M, Lim HH, Patrick JF, Anderson DJ and Lenarz T 2006 Electrophysiological validation of a human prototype auditory midbrain implant in a guinea pig model J. Assoc. Res. Otolaryngol 7 383–98 [PubMed: 17075701]

[14]. Lim HH, Lenarz M, Joseph G and Lenarz T 2013 Frequency representation within the human brain: stability versus plasticity Sci. Rep 3 1474 [PubMed: 23502431]

[15]. McKay CM, Lim HH and Lenarz T 2013 Temporal processing in the auditory system: insights from cochlear and auditory midbrain implantees J. Assoc. Res. Otolaryngol 14 103–24 [PubMed: 23073669]

[16]. Calixto R, Lenarz M, Neuheiser A, Scheper V, Lenarz T and Lim HH 2012 Co-activation of different neurons within an isofrequency lamina of the inferior colliculus elicits enhanced auditory cortical activation J. Neurophysiol 108 1199–210 [PubMed: 22623485]

[17]. Straka MM, Schendel D and Lim HH 2013 Neural integration and enhancement from the inferior colliculus up to different layers of auditory cortex J. Neurophysiol 110 1009–20 [PubMed: 23719210]

[18]. Schreiner CE and Langner G 1988 Periodicity coding in the inferior colliculus of the cat. II. topographical organization J. Neurophysiol 60 1823–40 [PubMed: 3236053]

[19]. Langner G, Albert M and Briede T 2002 Temporal and spatial coding of periodicity information in the inferior colliculus of awake chinchilla (*Chinchilla lanigera*) Hear. Res 168 110–30 [PubMed: 12117514]

[20]. Straka M, Schmitz S and Lim H 2014 Response features across the auditory midbrain reveal an organization consistent with a dual lemniscal pathway J. Neurophysiol doi:10.1152/jn.00008.2014

[21]. Semple MN and Aitkin LM 1979 Representation of sound frequency and laterality by units in central nucleus of cat inferior colliculus J. Neurophysiol 42 1626–39 [PubMed: 501392]

[22]. Wenstrup JJ, Ross LS and Pollak GD 1985 A functional organization of binaural responses in the inferior colliculus Hear. Res 17 191–5 [PubMed: 4008355]

[23]. Roth GL, Aitkin LM, Andersen RA and Merzenich MM 1978 Some features of the spatial organization of the central nucleus of the inferior colliculus of the cat J. Comp. Neurol 182 661–80 [PubMed: 721973]

[24]. Brückner S and Rubsamen R 1995 Binaural response characteristics in isofrequency sheets of the gerbil inferior colliculus Hear. Res 86 1–14 [PubMed: 8567406]

[25]. Stiebler I 1986 Tone-threshold mapping in the inferior colliculus of the house mouse Neurosci. Lett 65 336–40 [PubMed: 3520399]

[26]. Stiebler I and Ehret G 1985 Inferior colliculus of the house mouse. I. A quantitative study of tonotopic organization, frequency representation, and tone-threshold distribution J. Comp. Neurol 238 65–76 [PubMed: 4044904]

[27]. Hage S and Ehret G 2003 Mapping responses to frequency sweeps and tones in the inferior colliculus of house mice Eur. J. Neurosci 18 2301–12 [PubMed: 14622191]

[28]. Cant NB and Benson CG 2006 Organization of the inferior colliculus of the gerbil (*Meriones unguiculatus*): differences in distribution of projections from the cochlear nuclei and the superior olivary complex J. Comp. Neurol 495 511–28 [PubMed: 16498677]

[29]. Brunso-Bechtold JK, Thompson GC and Masterton RB 1981 HRP study of the organization of auditory afferents ascending to central nucleus of inferior colliculus in cat J. Comp. Neurol 197 705–22 [PubMed: 7229134]

[30]. Loftus WC, Bishop dc, Saint Marie RL and Oliver DL 2004 Organization of binaural excitatory and inhibitory inputs to the inferior colliculus from the superior olive J. Comp. Neurol 472 330–44 [PubMed: 15065128]

[31]. Oliver DL, Beckius GE, Bishop DC and Kuwada S 1997 Simultaneous anterograde labeling of axonal layers from lateral superior olive and dorsal cochlear nucleus in the inferior colliculus of cat J. Comp. Neurol 382 215–29 [PubMed: 9183690]

[32]. Shneiderman A and Henkel CK 1987 Banding of lateral superior olivary nucleus afferents in the inferior colliculus: a possible substrate for sensory integration J. Comp. Neurol 266 519–34 [PubMed: 2449472]

[33]. Cant NB and Benson CG 2007 Multiple topographically organized projections connect the central nucleus of the inferior colliculus to the ventral division of the medial geniculate nucleus in the gerbil, *Meriones unguiculatus* J. Comp. Neurol 503 432–53 [PubMed: 17503483]

[34]. Lim HH and Anderson DJ 2007 Spatially distinct functional output regions within the central nucleus of the inferior colliculus: implications for an auditory midbrain implant J. Neurosci 27 8733–43 [PubMed: 17687050]

[35]. Lim HH and Anderson DJ 2007 Antidromic activation reveals tonotopically organized projections from primary auditory cortex to the central nucleus of the inferior colliculus in guinea pig J. Neurophysiol 97 1413–27 [PubMed: 17151230]

[36]. Neuheiser A et al. 2010 Effects of pulse phase duration and location of stimulation within the inferior colliculus on auditory cortical evoked potentials in a guinea pig model J Assoc. Res. Otolaryngol 11 689–708 [PubMed: 20717834]

[37]. Wallace MN, Rutkowski RG and Palmer AR 2000 Identification and localisation of auditory areas in guinea pig cortex Exp. Brain Res 132 445–56 [PubMed: 10912825]

[38]. Redies H, Sieben U and Creutzfeldt OD 1989 Functional subdivisions in the auditory cortex of the guinea pig J. Comp. Neurol 282 473–88 [PubMed: 2723148]

[39]. Abeles M and Goldstein MH Jr 1970 Functional architecture in cat primary auditory cortex: columnar organization and organization according to depth J. Neurophysiol 33 172–87 [PubMed: 5411512]

[40]. Schreiner CE, Read HL and Sutter ML 2000 Modular organization of frequency integration in primary auditory cortex Annu. Rev. Neurosci 23 501–29 [PubMed: 10845073]

[41]. Schreiner CE and Sutter ML 1992 Topography of excitatory bandwidth in cat primary auditory cortex: single-neuron versus multiple-neuron recordings J. Neurophysiol 68 1487–502 [PubMed: 1479426]

[42]. Eggermont JJ and Roberts LE 2004 The neuroscience of tinnitus Trends Neurosci. 27 676–82 [PubMed: 15474168]

[43]. Muller-Preuss P and Mitzdorf U 1984 Functional anatomy of the inferior colliculus and the auditory cortex: current source density analyses of click-evoked potentials Hear. Res 16 133–42 [PubMed: 6526745]

[44]. Mitzdorf U 1985 Current source-density method and application in cat cerebral cortex: investigation of evoked potentials and EEG phenomena Physiol. Rev 65 37–100 [PubMed: 3880898]

[45]. Kral A, Hartmann R, Tillein J, Heid S and Klinke R 2000 Congenital auditory deprivation reduces synaptic activity within the auditory cortex in a layer-specific manner Cereb. Cortex 10 714–26 [PubMed: 10906318]

[46]. Huang CL and Winer JA 2000 Auditory thalamocortical projections in the cat: laminar and areal patterns of input J. Comp. Neurol 427 302–31 [PubMed: 11054695]

[47]. Smith PH and Populin LC 2001 Fundamental differences between the thalamocortical recipient layers of the cat auditory and visual cortices J. Comp. Neurol 436 508–19 [PubMed: 11447593]

[48]. Anderson DJ et al. 1989 Batch-fabricated thin-film electrodes for stimulation of the central auditory system IEEE Trans. Biomed. Eng 36 693–704 [PubMed: 2744793]

[49]. Snyder RL, Bierer JA and Middlebrooks JC 2004 Topographic spread of inferior colliculus activation in response to acoustic and intracochlear electric stimulation J. Assoc. Res. Otolaryngol 5 305–22 [PubMed: 15492888]

[50]. Malmierca MS, Rees A, Le Beau FE and Bjaalie JG 1995 Laminar organization of frequency-defined local axons within and between the inferior colliculi of the guinea pig J. Comp. Neurol 357 124–44 [PubMed: 7673462]

[51]. Schreiner CE and Langner G 1997 Laminar fine structure of frequency organization in auditory midbrain Nature 388 383–6 [PubMed: 9237756]

[52]. Malmierca MS et al. 2008 A discontinuous tonotopic organization in the inferior colliculus of the rat J. Neurosci 28 4767–76 [PubMed: 18448653]

[53]. Markovitz CD, Tang TT, Edge DP and Lim HH 2012 Threedimensional brain reconstruction of *in vivo* electrode tracks for neuroscience and neural prosthetic applications Front. Neural Circuits 6 39 [PubMed: 22754502]

[54]. Syka J, Popelar J, Kvasnak E and Astl J 2000 Response properties of neurons in the central nucleus and external and dorsal cortices of the inferior colliculus in guinea pig Exp. Brain Res 133 254–66 [PubMed: 10968227]

[55]. Mendelson J, Schreiner CE and Sutter ML 1997 Functional topography of cat primary auditory cortex: response latencies J. Comp. Physiol. A 181 615–33 [PubMed: 9449822]

[56]. Team RCR 2013 A Language and Environment for Statistical Computing (Vienna: R Foundation for Statistical Computing)

[57]. Eggermont JJ and Smith GM 1995 Synchrony between single-unit activity and local field potentials in relation to periodicity coding in primary auditory cortex J. Neurophysiol 73 227–45 [PubMed: 7714568]

[58]. Humphrey D and Schmidt E 1991 Extracellular single-unit recording methods Neurophysiological Techniques. Neuromethods vol 15 ed Boulton A, Baker G and Vanderwolf C (NewYork: Humana) pp 1–64

[59]. Leung L-WS 1990 Field potentials in the central nervous system Neurophysiological Techniques. Neuromethods vol 15 ed Boulton A, Baker G and Vanderwolf C (NewYork: Humana) pp 277–312

[60]. Wehr M and Zador AM 2005 Synaptic mechanisms of forward suppression in rat auditory cortex Neuron 47 437–45 [PubMed: 16055066]

[61]. Astl J, Popelar J, Kvasnak E and Syka J 1996 Comparison of response properties of neurons in the inferior colliculus of guinea pigs under different anesthetics Audiology 35 335–45 [PubMed: 9018367]

[62]. Syka J, Suta D and Popelar J 2005 Responses to species-specific vocalizations in the auditory cortex of awake and anesthetized guinea pigs Hear. Res 206 177–84 [PubMed: 16081007]

[63]. Zurita P, Villa AE, de Ribaupierre Y, de Ribaupierre F and Rouiller EM 1994 Changes of single unit activity in the cat's auditory thalamus and cortex associated to different anesthetic conditions Neurosci. Res 19 303–16 [PubMed: 8058206]

[64]. Wang X, Lu T, Snider RK and Liang L 2005 Sustained firing in auditory cortex evoked by preferred stimuli Nature 435 341–6 [PubMed: 15902257]

[65]. Kirby AE and Middlebrooks JC 2012 Unanesthetized auditory cortex exhibits multiple codes for gaps in cochlear implant pulse trains J. Assoc. Res. Otolaryngol 13 67–80 [PubMed: 21969022]

[66]. Kisley MA and Gerstein GL 1999 Trial-to-trial variability and state-dependent modulation of auditory-evoked responses in cortex J. Neurosci 19 10451–60 [PubMed: 10575042]

[67]. Rennaker RL, Carey HL, Anderson SE, Sloan AM and Kilgard MP 2007 Anesthesia suppresses nonsynchronous responses to repetitive broadband stimuli Neuroscience 145 357–69 [PubMed: 17207583]

[68]. Eggermont JJ 1992 Stimulus induced and spontaneous rhythmic firing of single units in cat primary auditory cortex Hear. Res 61 1–11 [PubMed: 1526882]

[69]. Winer JA and Prieto JJ 2001 Layer V in cat primary auditory cortex (AI): cellular architecture and identification of projection neurons J. Comp. Neurol 434 379–412 [PubMed: 11343289]

[70]. Sherman SM 2001 Tonic and burst firing: dual modes of thalamocortical relay Trends Neurosci. 24 122–6 [PubMed: 11164943]

[71]. Swadlow HA and Gusev AG 2001 The impact of 'bursting' thalamic impulses at a neocortical synapse Nat. Neurosci 4 402–8 [PubMed: 11276231]

[72]. Usrey WM, Alonso JM and Reid RC 2000 Synaptic interactions between thalamic inputs to simple cells in cat visual cortex J. Neurosci 20 5461–7 [PubMed: 10884329]

[73]. He J and Hu B 2002 Differential distribution of burst and single-spike responses in auditory thalamus J. Neurophysiol 88 2152–6 [PubMed: 12364537]

[74]. Hu B 1995 Cellular basis of temporal synaptic signalling: an *in vitro* electrophysiological study in rat auditory thalamus J. Physiol 483 167–82 [PubMed: 7776230]

[75]. Lee CC 2012 Thalamic and cortical pathways supporting auditory processing Brain Lang. 126 22–8 [PubMed: 22728130]

[76]. Cetas JS, de Venecia RK and McMullen NT 1999 Thalamocortical afferents of lorente de no: medial geniculate axons that project to primary auditory cortex have collateral branches to layer I Brain Res. 830 203–8 [PubMed: 10350577]

[77]. Mitani A, Shimokouchi M, Itoh K, Nomura S, Kudo M and Mizuno N 1985 Morphology and laminar organization of electrophysiologically identified neurons in the primary auditory cortex in the cat J. Comp. Neurol 235 430–47 [PubMed: 3998218]

[78]. Winer JA 2010 A profile of auditory forebrain connections and circuits The Auditory Cortex ed Winer JA and Schreiner CE (New York: Springer) pp 41–74

[79]. Moeller CK, Kurt S, Happel MF and Schulze H 2010 Long-range effects of GABAergic inhibition in gerbil primary auditory cortex Eur. J. Neurosci 31 49–59 [PubMed: 20092555]

[80]. Markovitz CD, Tang TT and Lim HH 2013 Tonotopic and localized pathways from primary auditory cortex to the central nucleus of the inferior colliculus Front. Neural Circuits 7 77 [PubMed: 23641201]

[81]. Heffner R, Heffner H and Masterton B 1971 Behavioral easurements of absolute and frequency-difference thresholds in guinea pig J. Acoust. Soc. Am 49 1888–95 [PubMed: 5125738]

[82]. Prosen CA, Petersen M, Moody DB and Stebbins WC 1978 Auditory thresholds and kanamycin-induced hearing loss in the guinea pig assessed by a positive reinforcement procedure J. Acoust. Soc. Am 63 559–66 [PubMed: 670552]

[83]. Rodrigues-Dagaeff C, Simm G, De Ribaupierre Y, Villa A, De Ribaupierre F and Rouiller EM 1989 Functional organization of the ventral division of the medial geniculate body of the cat: evidence for a rostro-caudal gradient of response properties and cortical projections Hear. Res 39 103–25 [PubMed: 2737959]

[84]. Morel A and Imig TJ 1987 Thalamic projections to fields A, AI, P, and VP in the cat auditory cortex J. Comp. Neurol 265 119–44 [PubMed: 2826552]

[85]. Storace DA, Higgins NC and Read HL 2010 Thalamic label patterns suggest primary and ventral auditory fields are distinct core regions J. Comp. Neurol 518 1630–46 [PubMed: 20232478]

[86]. Polley DB, Read HL, Storace DA and Merzenich MM 2007 Multiparametric auditory receptive field organization across five cortical fields in the albino rat J. Neurophysiol 97 3621–38 [PubMed: 17376842]

[87]. Storace DA, Higgins NC, Chikar JA, Oliver DL and Read HL 2012 Gene expression identifies distinct ascending glutamatergic pathways to frequency-organized auditory cortex in the rat brain J. Neurosci 32 15759–68 [PubMed: 23136415]

[88]. Schreiner C, Froemke R and Atencio C 2011 Spectral processing in auditory cortex The Auditory Cortex ed Winer JA and Schreiner CE (Berlin: Springer) pp 275–308

[89]. Allitt BJ, Benjaminsen C, Morgan SJ and Paolini AG 2013 Intralaminar stimulation of the inferior colliculus facilitates frequency-specific activation in the auditory cortex J. Neural Eng 10 046008 [PubMed: 23800787]

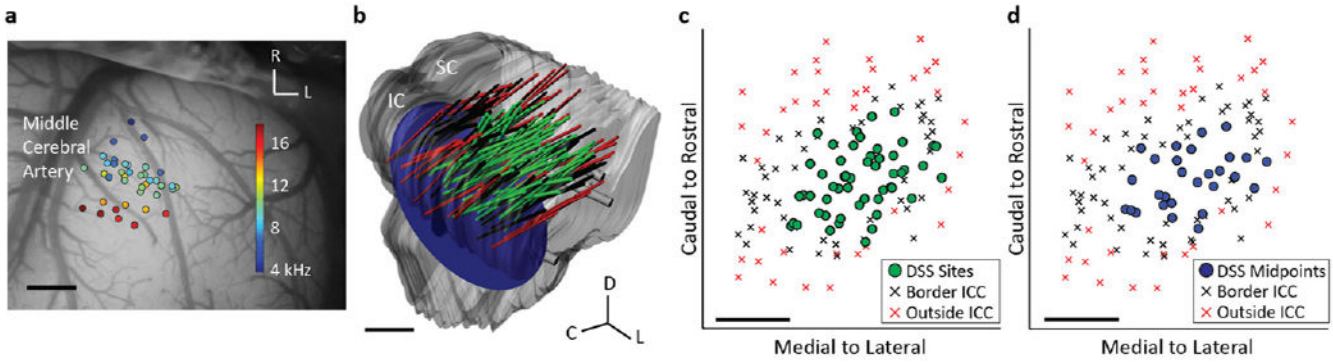

Figure 1.

(a) The A1 recording locations, overlaid on a typical guinea pig cortex, with color representing the BF for each location averaged across layers I–V. Only sites that were BF-matched to ICC pairs were included and analyzed. (b) The midbrain and array placements were reconstructed in three dimensions and normalized onto a single brain. Green shanks correspond to ICC placements which were electrically stimulated (in pairs). Black and red shanks are placements on the border of or outside the ICC, as determined by FRMs along the shank (see Results). The 10 kHz isofrequency lamina was approximated by a plane at a depth which corresponds to neurons with 10 kHz BF, the average BF of the stimulated ICC sites. (c) The locations of the stimulated sites in the ICC were plotted along with the border and outside ICC sites across the 10 kHz lamina. (d) Analysis of the location effects across an ICC lamina was performed by determining the midpoint between each stimulated pair of ICC neurons. Scale bars are 1 mm. A1, primary auditory cortex; BF, best frequency; ICC, central nucleus of the inferior colliculus; SC, superior colliculus; IC, inferior colliculus; D, dorsal; C, caudal; L, lateral; R, rostral.

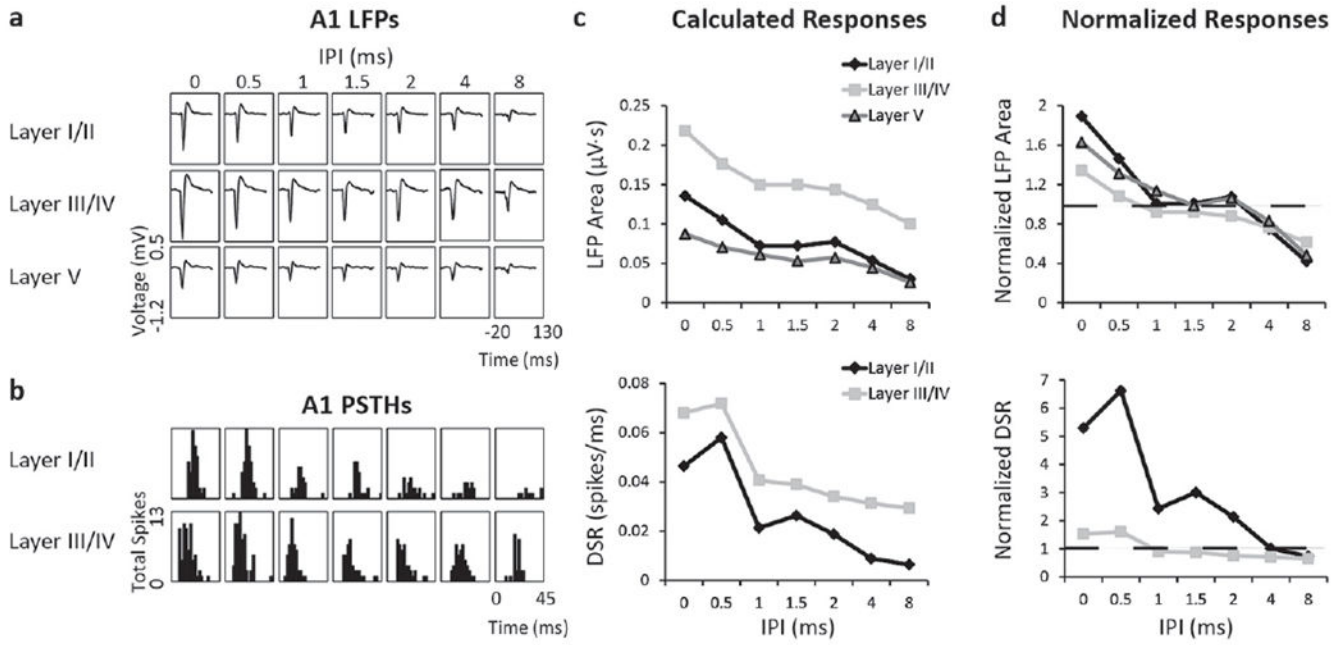

Figure 2.

A comparison of LFP and spiking responses measured simultaneously across different layers of a single A1 shank for one stimulation case within one animal in response to one stimulation level. While greater responses at shorter IPIs were observed at all layers, the most enhancement for both LFPs and DSRs was observed in layer I/II. (a) Recorded in layers I/II (top), III/IV (middle) and V (bottom) of A1, LFPs increase in response to DSS as IPIs decrease from 8 to 0 ms (right to left columns). (b) PSTHs recorded in layers I/II and III/IV of A1 in response to DSS at IPIs from 0 to 8 ms. (c) LFP areas and DSRs were calculated for each layer of A1. (d) For the different layers, IPI curves were created by normalizing cortical responses to the sum of responses to individual pulses. The normalization factor 1 is indicated by the dashed line. Electrical artifacts were removed in A and B. Time is relative to initial stimulus onset. DSR, driven spike rate; LFP, local field potential; IPI, inter-pulse interval; PSTH, post-stimulus time histogram.

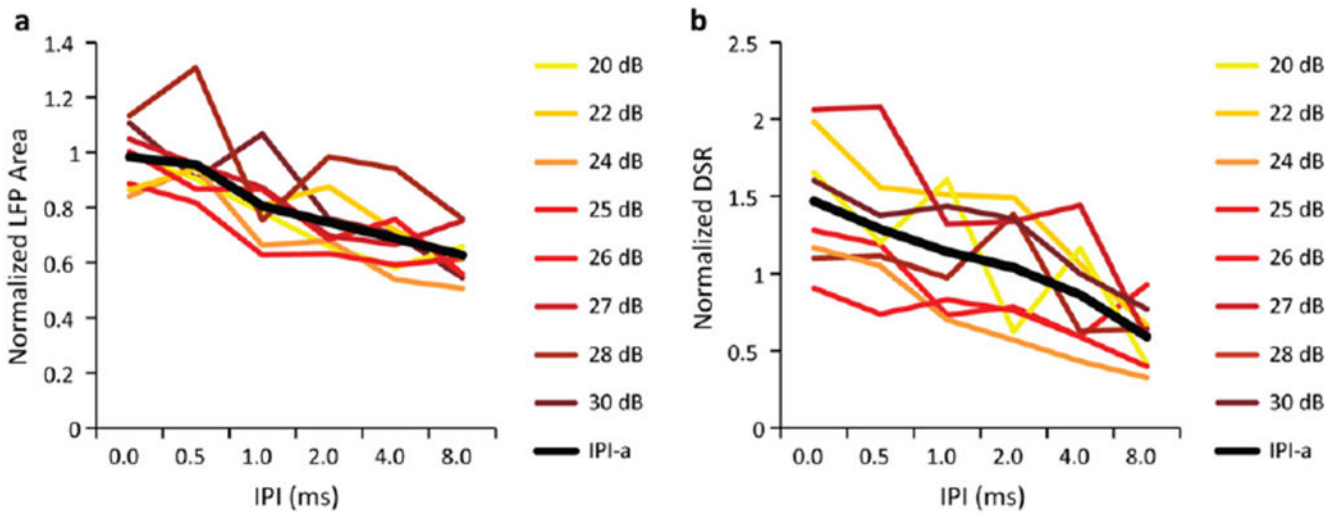

Figure 3.

The effects of different stimulation levels on the normalized LFP (a) and DSR (b) responses recorded in layer III/IV of A1 in response to DSS applied at a single ICC pair. One ICC site from the pair was stimulated at the level indicated in each plot while the other ICC site was stimulated at a constant level. The IPI curves were averaged across the stimulation levels to calculate the IPI-a curves, shown in black in each panel. Only levels that were above threshold and below saturation were analyzed. Though some differences could be observed between curves across levels, there were no obvious or consistent trends across levels for either the normalized LFP or DSR data.

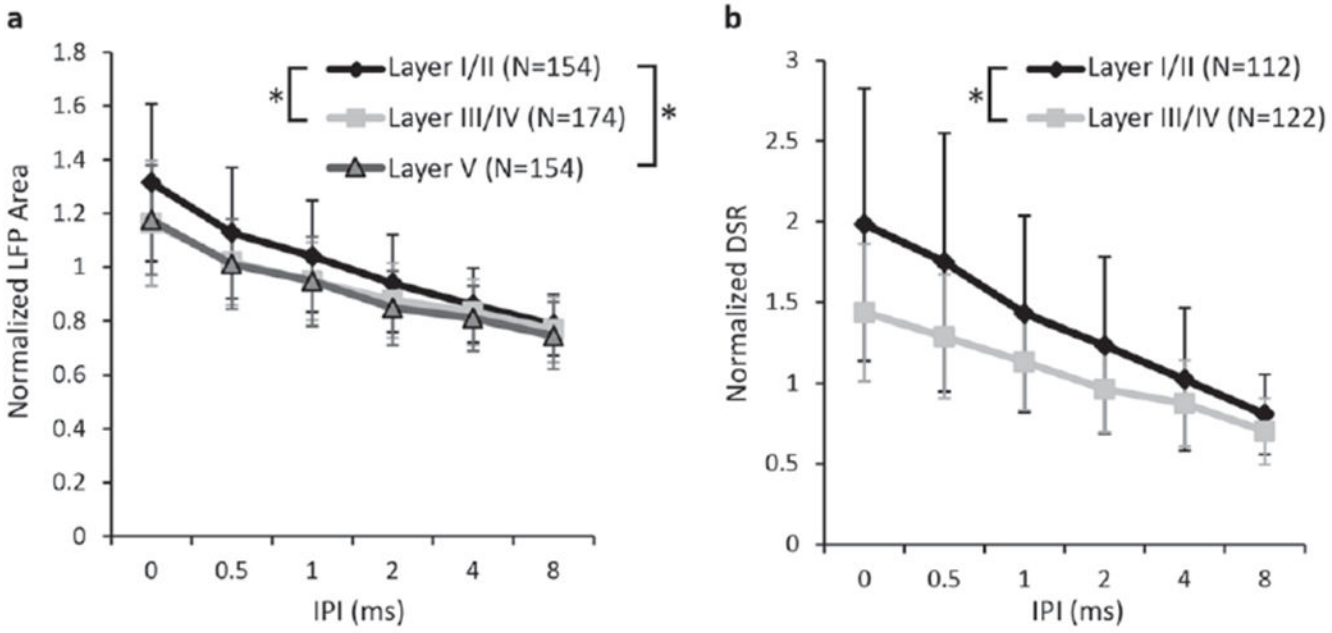

Figure 4.

Summary of LFP (a) and DSR (b) responses across A1 layers, averaged across all stimulation cases and animals (*N* = number of stimulation cases). For IPIs between 0–4 ms for LFP areas and 0–8 ms for DSRs, activity in layer I/II was significantly increased above the deeper layers (marked by asterisks; see text for *P*-values).

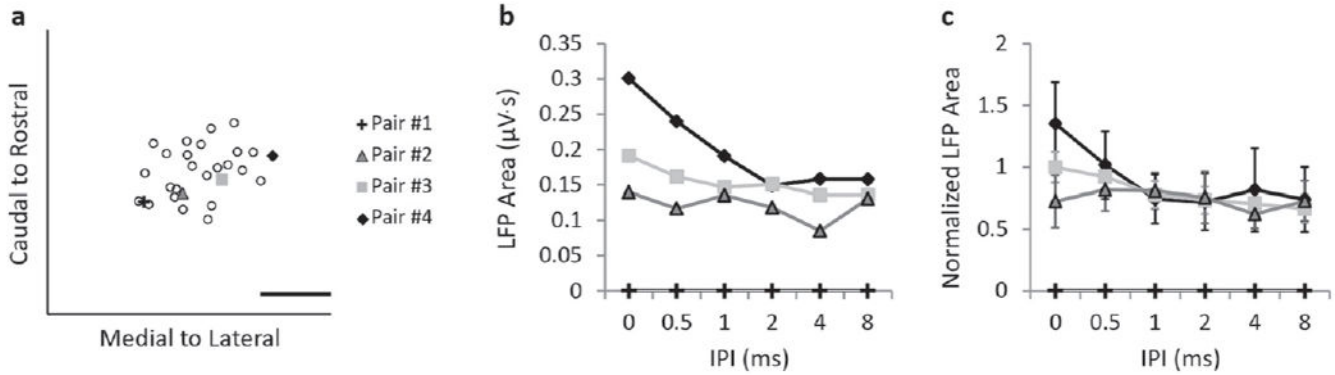

Figure 5.

A case example of how stimulating different locations across an ICC isofrequency lamina alters IPI and IPI-a curves recorded in one cortical location from a single animal. (a) The midpoint locations of four pairs of ICC sites stimulated across the ICC lamina are shown with other ICC midpoint locations for reference. Elicited activity was recorded in one cortical location in layer III/IV. (b) For pair #2–4, we found stimulation levels that elicited similar cortical activity at the 8 ms IPI and found that LFP areas increased more at shorter IPIs with more rostral–lateral stimulation locations. Stimulating pair #1 did not result in reliable LFP areas for this cortical location within the threshold bounds of our electrode arrays. (c) When averaged across stimulation levels, the IPI-a curves confirm that more rostral locations reveal higher levels of cortical activity. Error bars are standard deviations across levels. The scale bar is 1 mm.

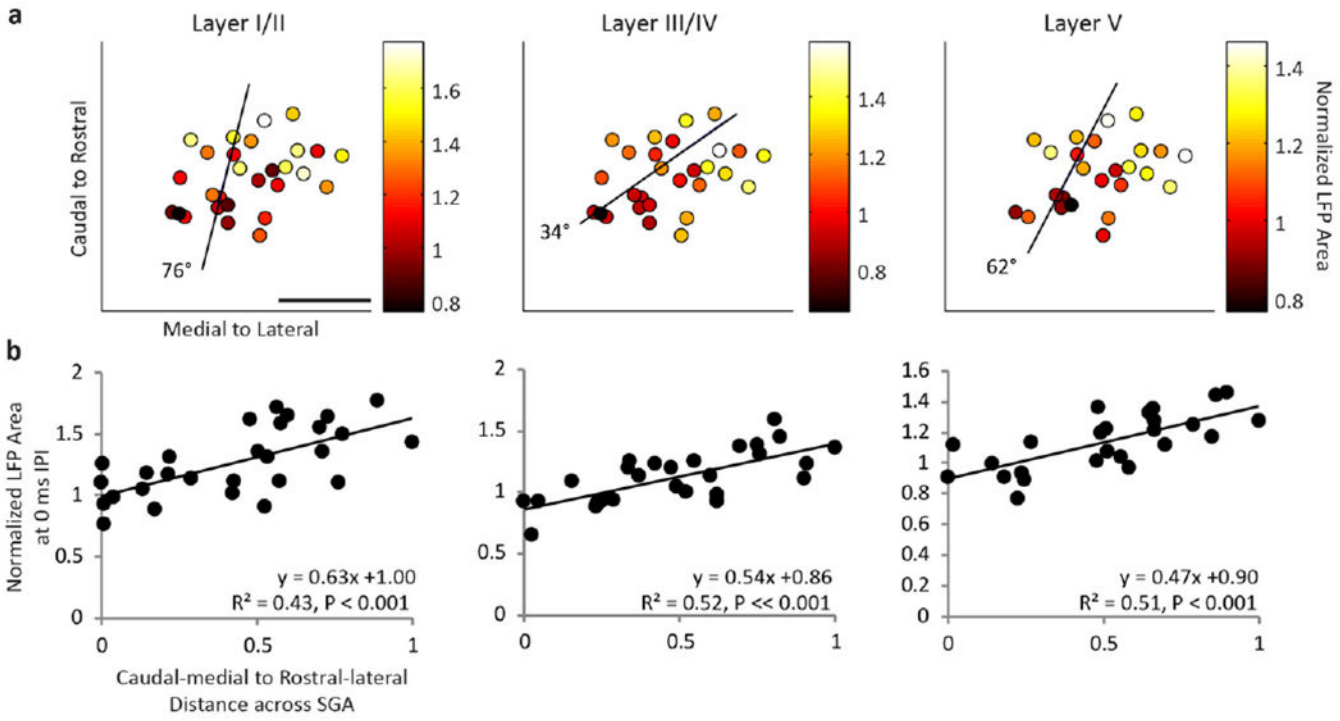

Figure 6.

DSS in rostral–lateral ICC elicits greater normalized LFP areas across cortical layers than caudal–medial regions. (a) The amount of elicited normalized LFP area (color) is shown for the midpoint location between each pair of stimulated ICC sites (dots) at the 0 ms IPI. Cortical activity was averaged across A1 locations within a specific layer if multiple locations recorded activity elicited from one pair of sites. Using multiple linear regression to fit the cortical activity as a function of the ICC midpoint location, the steepest gradient axis (line) was found. The angle of the steepest gradient is shown, where 0 would indicate alignment with the medial to lateral axis and 90° would indicate alignment with the caudal to rostral axis. The scale bar is 1 mm. (b) Normalized LFP area is shown as a function of midpoint location along the steepest gradient axis, where 0 is the most caudal–medial location and 1 is the most rostral–lateral location. SGA: steepest gradient axis.

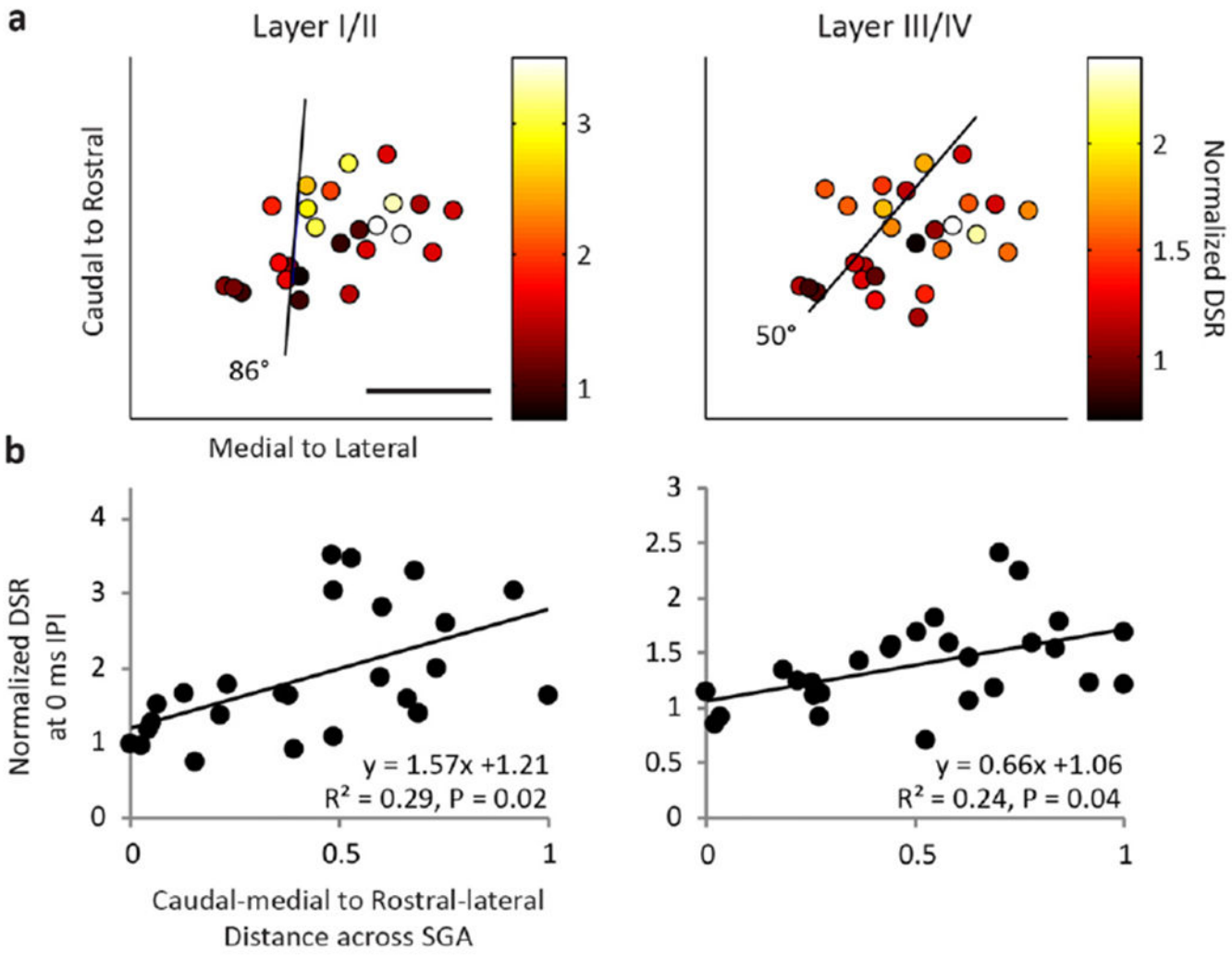

Figure 7.

(a) Normalized DSRs (color) recorded in supragranular and granular layers of the cortex are shown for the midpoint between each stimulation location. (b) Normalized DSR is plotted as a function of the midpoint location across the steepest gradient axis ((a) black line). Similar to figure 6, DSS of rostral–lateral areas results in greater normalized DSR activity than caudal–medial areas. The scale bar is 1 mm.

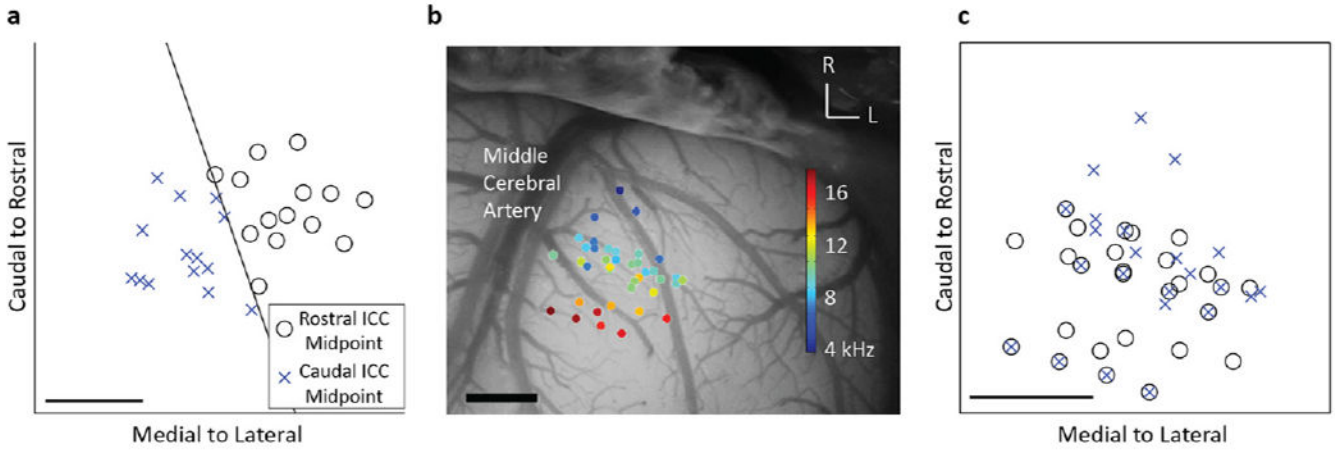

Figure 8.

The ICC lamina was split into caudal–medial versus rostral–lateral regions (a) by the line perpendicular to the average steepest gradient axis, which is the average direction where cortical activity varies the most for the 0 and 0.5 ms IPI. The midpoint between each stimulation pair was determined to originate from one of those two regions. The A1 locations, overlaid on the cortex with BF values (b), recorded activity elicited from the caudal–medial region similar to those of the rostral–lateral region (c). The scale bars are 1 mm. Note that panels with A1 locations are boxed while ICC locations are open.

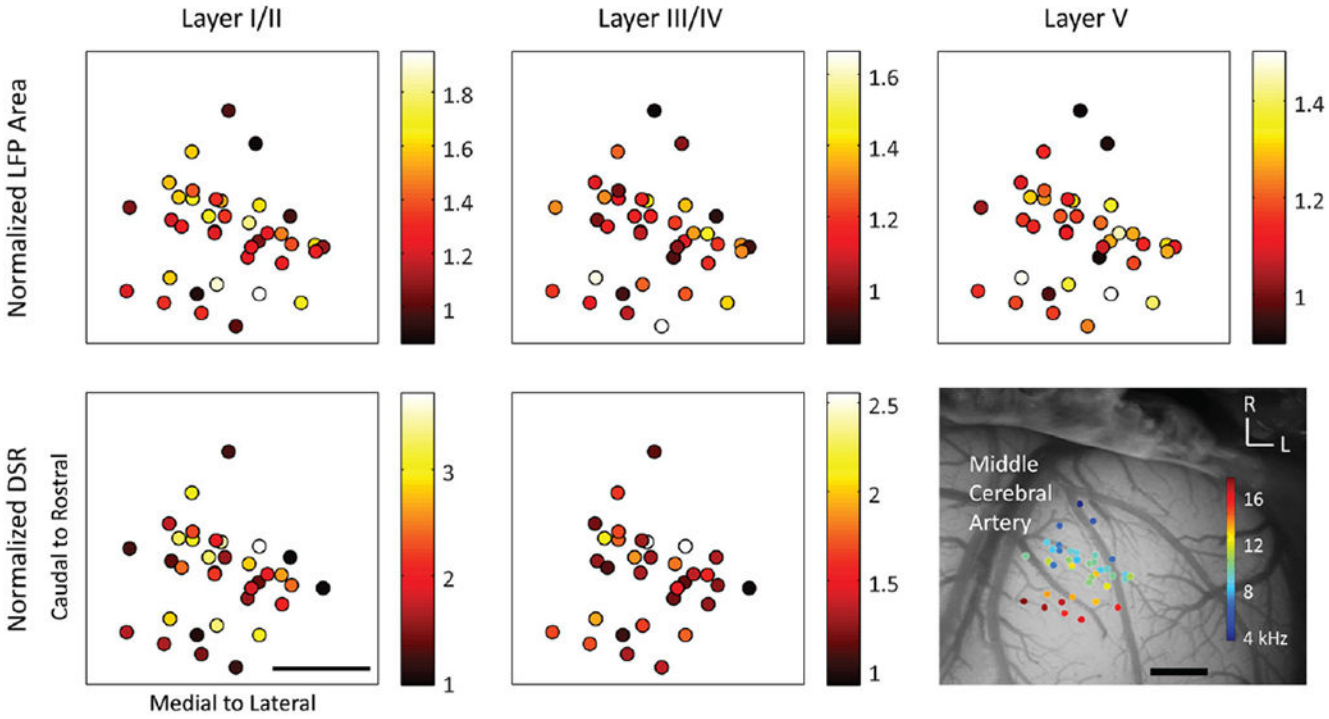

Figure 9.

The location of sites across A1 does not have a clear impact on the amount of normalized LFP area (top) or DSRs (bottom) recorded across different layers (columns). Indicated by color (no units), the normalized cortical activity for each location was averaged across stimulated locations in the ICC. The scale bars are 1 mm.

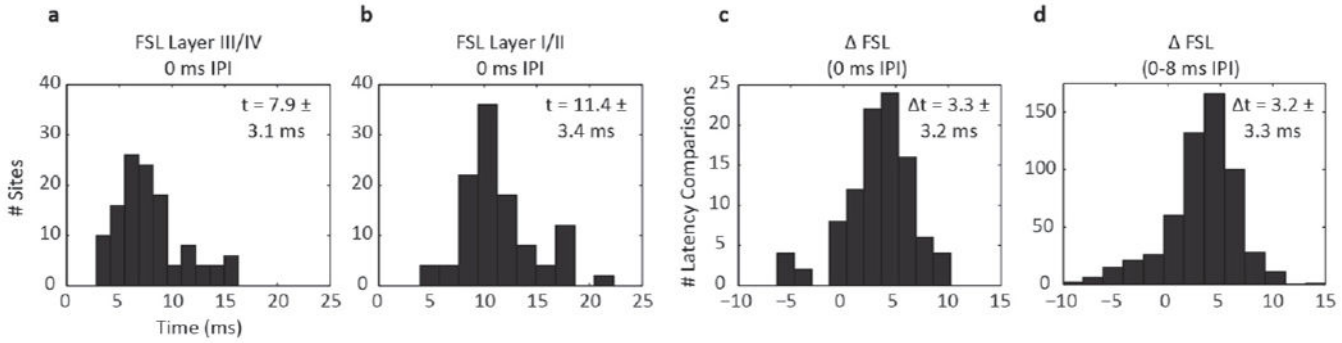

Figure 10.

Histograms of FSLs for all stimulation cases recorded in layer III/IV (a) and layer I/II (b) at the 0 ms IPI. When comparing sites recorded from the same A1 location, FSLs recorded in layer I/II were on average ~3 ms longer than those in layer III/IV at the 0 ms IPI (c) as well as all IPIs from 0–8 ms (d).

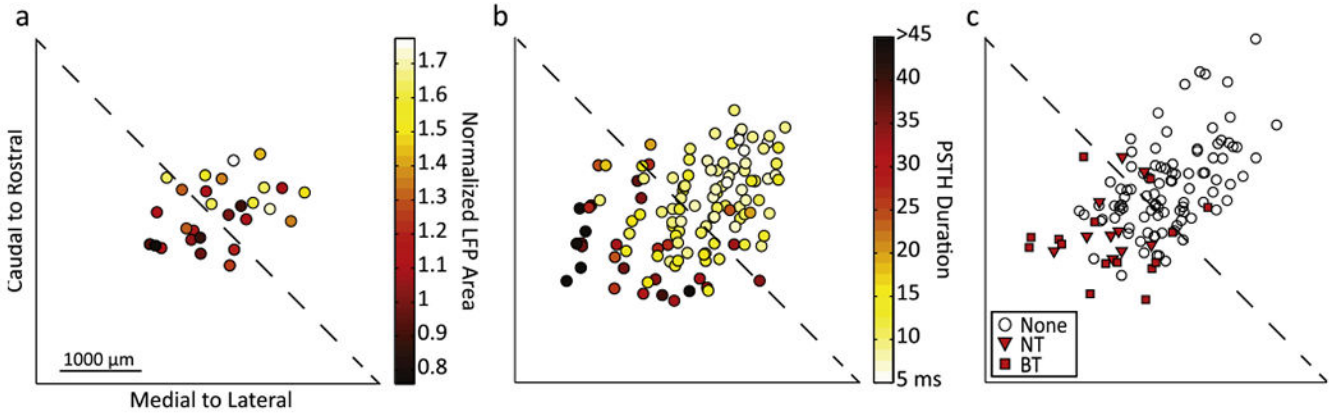

Figure 11.

Comparisons across different experiments show that caudal–medial regions exhibit different response properties than rostral–lateral ICC regions in locations which, when electrically stimulated, elicit different cortical responses. (a) Normalized LFPs recorded in layer I/II (color) were typically smaller in the caudal–medial region and enhanced in rostral–lateral region across the 10 kHz isofrequency lamina of the ICC. (b) In response to 10 kHz pure tones (0.5 ms), the duration of PSTHs were longer in the caudal–medial region and shorter in the rostral–lateral region across the 10 kHz isofrequency lamina of the ICCs (data originally presented in Straka *et al* [20]). (c) A1 stimulation caused excitatory responses in the caudal–medial but not the rostral–lateral region of the ICC for sites with BFs of 10–16 kHz (data originally presented in Markovitz *et al* [80]). These excitatory responses could be present across a few or many frequency laminae (i.e., broadly tuned (BT) or narrowly tuned (NT), respectively). Locations from (a), (b), and (c) were normalized in the same standard brain and locations were taken across the 10 kHz lamina.